

Analysis of thermal processes occurring in heated multilayered metal films using the dual-phase lag model

E. MAJCHRZAK, G. KAŁUŻA

*Institute of Computational Mechanics and Engineering
Silesian University of Technology
Konarskiego 18a
44-100 Gliwice, Poland
e-mails: ewa.majchrzak@polsl.pl, grazyna.kaluza@polsl.pl*

A MULTILAYERED THIN METAL FILM subjected to an ultra-short laser pulse is considered. A mathematical description of the discussed process is based on the system of the dual-phase lag equations supplemented by appropriate boundary and initial conditions. Special attention is devoted to the ideal contact conditions at the interfaces between the layers, which in the case of the dual-phase lag model must be formulated in a different way than in the macroscopic Fourier model. To solve the problem the explicit scheme of the finite difference method is developed. In the final part of the paper the example of computations is shown.

Key words: multilayered thin metal films, dual-phase lag equation, FDM.

Copyright © 2017 by IPPT PAN

1. Introduction

ONE OF THE MODELS DESCRIBING THE THERMAL PROCESSES occurring in thin metal films subjected to an ultra-short laser pulse is the dual-phase lag equation [1–6]

$$(1.1) \quad x \in \Omega : \quad c \left[\frac{\partial T(x, t)}{\partial t} + \tau_q \frac{\partial^2 T(x, t)}{\partial t^2} \right] = \nabla \left[\lambda \nabla T(x, t) \right] \\ + \tau_T \nabla \left[\lambda \frac{\partial \nabla T(x, t)}{\partial t} \right] + Q(x, t) + \tau_q \frac{\partial Q(x, t)}{\partial t},$$

where $T(x, t)$ is the temperature, c is the volumetric specific heat, λ is the thermal conductivity, τ_q is the relaxation time, τ_T is the thermalization time and $Q(x, t)$ is the source function connected with the laser heating.

This equation can be derived when the following formula is introduced in place of the classical Fourier law $\mathbf{q}(x, t) = -\lambda \nabla T(x, t)$:

$$(1.2) \quad \mathbf{q}(x, t + \tau_q) = -\lambda \nabla T(x, t + \tau_T),$$

where ∇T is the temperature gradient and \mathbf{q} is the heat flux.

Using the Taylor series expansions the following first-order approximation of equation (1.2) can be accepted

$$(1.3) \quad \mathbf{q}(x, t) + \tau_q \frac{\partial \mathbf{q}(x, t)}{\partial t} = -\lambda \left[\nabla T(x, t) + \tau_T \frac{\partial \nabla T(x, t)}{\partial t} \right].$$

In the case of multilayered domains, the system of equations of type (1.1) for each subdomain should be taken into account and on the contact surfaces the appropriate boundary conditions should be assumed. In the case of ideal contact these boundary conditions take the following form:

$$(1.4) \quad x \in \Gamma_e : \quad \begin{cases} T_e(x, t) = T_{e+1}(x, t), \\ q_e(x, t) = q_{e+1}(x, t), \end{cases} \quad e = 1, 2, \dots, E - 1.$$

Using the relationship (1.3) between the heat flux and temperature gradient, the second part of boundary condition (1.4) should be properly formulated.

It should be noted that in the literature different ways of modeling of ideal contact condition (1.4) are presented. For example, at the stage of computations, the FDM grid in which the nodes are located not on the contact surface but at a certain distance from this surface is introduced [7–9]. Another approach is to use the staggered grid where the ‘temperature nodes’ and ‘heat flux nodes’ are distinguished separately, e.g., [10, 11]. Finally, in several articles (e.g. [12, 13]), the condition of ideal contact is formulated in the same manner as in the case of macroscopic Fourier model, which is, of course, a significant simplification.

In this paper, the second part of interfacial condition (1.4) is expressed in terms of temperature. This allows to introduce the spatial grid with the nodes located on the contact surface. The aim of the study is also to compare the results of computations for different ways of ideal contact condition modeling. Thus, in Section 2 the mathematical model of thermal processes in the multilayered thin metal film subjected to the ultrashort laser pulse is presented. Section 3 presents the boundary condition of ideal contact, which takes into account the relationship (1.3) between the heat flux and temperature gradient. The explicit scheme of the finite difference method is presented in Section 4. The FDM algorithm constitutes a basis for an ‘in house’ computer program used at the stage of numerical modeling (Section 5). In the final part of the paper the conclusions are formulated.

2. Governing equations

A multilayered thin film of thickness $L = L_1 + L_2 + \dots + L_E$, as shown in Fig. 1, with an initial temperature distribution $T(x, 0) = T_p$ is considered. The constant thermal properties of successive layers and the ideal thermal contact between the layers are assumed.

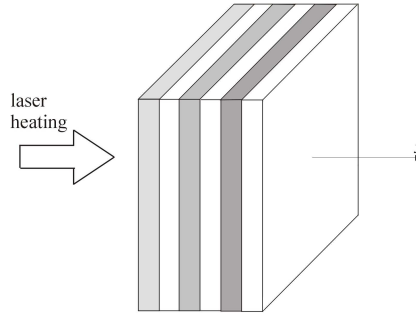


FIG. 1. Multilayered thin metal film.

The temperature distribution in the successive layers is described by the system of equations (1D problem) [7, 8]:

$$(2.1) \quad L_{e-1} < x < L_e : \quad \frac{\partial T_e(x, t)}{\partial t} + \tau_{qe} \frac{\partial^2 T_e(x, t)}{\partial t^2} = a_e \frac{\partial^2 T_e(x, t)}{\partial x^2} + \tau_{Te} a_e \frac{\partial^3 T_e(x, t)}{\partial t \partial x^2} + \frac{1}{c_e} Q_e(x, t) + \frac{\tau_{qe}}{c_e} \frac{\partial Q_e(x, t)}{\partial t}, \quad e = 1, 2, \dots, E,$$

where $a_e = \lambda_e/c_e$ (λ_e is the thermal conductivity of e -th layer, c_e is the volumetric specific heat), τ_{qe} is the relaxation time, τ_{Te} is the thermalization time, T_e is the temperature, x is the spatial coordinate and t is the time.

A front surface $x = L_0 = 0$ is irradiated by a laser pulse and the source function $Q_1(x, t)$ connected with the laser heating is defined as follows [14]:

$$(2.2) \quad Q_1(x, t) = \sqrt{\frac{\beta}{\pi}} \frac{1 - R_1}{t_p \delta_1} I_0 \exp\left[-\frac{x}{\delta_1} - \beta \frac{(t - 2t_p)^2}{t_p^2}\right],$$

where I_0 is the laser intensity, t_p is the characteristic time of a laser pulse, δ_1 is the absorption depth, $x \leq \delta_1 < L_1$, R_1 is the reflectivity of the irradiated surface and $\beta = 4 \ln 2$. For $e = 2, 3, \dots, E$: $Q_e(x, t) = 0$.

Introducing the source function (2.2) allows to assume for $x = 0$ and $x = L$ the no-flux conditions, namely [14]:

$$(2.3) \quad q_1(0, t) = 0, \quad q_E(L, t) = 0.$$

The boundary conditions on the contact surfaces between subdomains have the form of continuity ones, this means that

$$(2.4) \quad x = L_e : \quad \begin{cases} T_e(x, t) = T_{e+1}(x, t), \\ q_e(x, t) = q_{e+1}(x, t), \end{cases} \quad e = 1, 2, \dots, E - 1.$$

The initial conditions ($t = 0$) are also given

$$(2.5) \quad \begin{aligned} t = 0 : \quad & T_e(x, 0) = T_p, \\ x \leq \delta_1 : \quad & \left. \frac{\partial T_1(x, t)}{\partial t} \right|_{t=0} = \frac{Q_1(x, 0)}{c_1}, \\ x > \delta_1 : \quad & \left. \frac{\partial T_e(x, t)}{\partial t} \right|_{t=0} = 0. \end{aligned}$$

One can see that the initial heating rate is defined in different ways for $x \leq \delta_1$ and for $x > \delta_1$. It results from the assumption that the internal heat source connected with the laser radiation acts only in the layer of thickness δ_1 corresponding to the absorption depth.

3. Interfacial condition

From the numerical point of view, it is convenient to express the ideal contact condition (2.4) in terms of temperature. For this purpose, the following relationship between the heat flux and temperature gradient must be applied (cf. formula (1.3)):

$$(3.1) \quad q_e(x, t) + \tau_{qe} \frac{\partial q_e(x, t)}{\partial t} = -\lambda_e \left[\frac{\partial T_e(x, t)}{\partial x} + \tau_{Te} \frac{\partial^2 T_e(x, t)}{\partial t \partial x} \right].$$

The dependence (3.1) is differentiated with respect to time and then multiplied by τ_{qe+1}

$$(3.2) \quad \begin{aligned} \tau_{qe+1} \frac{\partial}{\partial t} \left[q_e(x, t) + \tau_{qe} \frac{\partial q_e(x, t)}{\partial t} \right] \\ = -\lambda_e \tau_{qe+1} \frac{\partial}{\partial t} \left[\frac{\partial T_e(x, t)}{\partial x} + \tau_{Te} \frac{\partial^2 T_e(x, t)}{\partial t \partial x} \right]. \end{aligned}$$

Adding the sides of equations (3.1) and (3.2) gives

$$(3.3) \quad \begin{aligned} q_e(x, t) + (\tau_{qe} + \tau_{qe+1}) \frac{\partial q_e(x, t)}{\partial t} + \tau_{qe} \tau_{qe+1} \frac{\partial^2 q_e(x, t)}{\partial t^2} \\ = -\lambda_e \left[\frac{\partial T_e(x, t)}{\partial x} + \tau_{Te} \frac{\partial^2 T_e(x, t)}{\partial t \partial x} \right] - \lambda_e \tau_{qe+1} \frac{\partial}{\partial t} \left[\frac{\partial T_e(x, t)}{\partial x} + \tau_{Te} \frac{\partial^2 T_e(x, t)}{\partial t \partial x} \right]. \end{aligned}$$

In a similar way one obtains

$$(3.4) \quad \begin{aligned} q_{e+1}(x, t) + (\tau_{qe} + \tau_{qe+1}) \frac{\partial q_{e+1}(x, t)}{\partial t} + \tau_{qe} \tau_{qe+1} \frac{\partial^2 q_{e+1}(x, t)}{\partial t^2} \\ = -\lambda_{e+1} \left[\frac{\partial T_{e+1}(x, t)}{\partial x} + \tau_{Te+1} \frac{\partial^2 T_{e+1}(x, t)}{\partial t \partial x} \right] \\ - \lambda_{e+1} \tau_{qe} \frac{\partial}{\partial t} \left[\frac{\partial T_{e+1}(x, t)}{\partial x} + \tau_{Te+1} \frac{\partial^2 T_{e+1}(x, t)}{\partial t \partial x} \right]. \end{aligned}$$

Taking into account the second part of condition (2.4) it can be seen that the left-hand sides of equations (3.3) and (3.4) are the same. Thus the right-hand sides of these equations are created equal

$$\begin{aligned}
 (3.5) \quad & -\lambda_e \frac{\partial T_e(x, t)}{\partial x} - \lambda_e(\tau_{Te} + \tau_{qe+1}) \frac{\partial^2 T_e(x, t)}{\partial t \partial x} - \lambda_e \tau_{Te} \tau_{qe+1} \frac{\partial^3 T_e(x, t)}{\partial t^2 \partial x} \\
 & = -\lambda_{e+1} \frac{\partial T_{e+1}(x, t)}{\partial x} - \lambda_{e+1}(\tau_{Te+1} + \tau_{qe}) \frac{\partial^2 T_{e+1}(x, t)}{\partial t \partial x} \\
 & \quad - \lambda_{e+1} \tau_{Te+1} \tau_{qe} \frac{\partial^3 T_{e+1}(x, t)}{\partial t^2 \partial x}.
 \end{aligned}$$

The final form of the above designated condition (3.5) corresponds to the formula presented in [15].

It should be noted that in the case of Neumann boundary conditions (2.3) one has (cf. formula (3.1))

$$\begin{aligned}
 (3.6) \quad & \left[\frac{\partial T_1(x, t)}{\partial x} + \tau_{T1} \frac{\partial^2 T_1(x, t)}{\partial t \partial x} \right]_{x=0} = 0, \\
 & \left[\frac{\partial T_E(x, t)}{\partial x} + \tau_{TE} \frac{\partial^2 T_E(x, t)}{\partial t \partial x} \right]_{x=L} = 0.
 \end{aligned}$$

4. Method of solution

At the stage of numerical computations the finite difference method is proposed. A geometrical mesh is shown in Fig. 2.

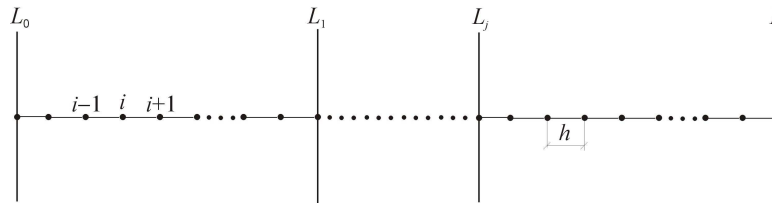


FIG. 2. Geometrical mesh.

Let $T_i^f = T(x_i, f\Delta t)$ where Δt is the time step, $x_i = ih$ (h is the mesh step) and $f = 0, 1, \dots, F$. Taking into account the initial conditions (2.5) one has

$$T_i^0 = T_p, \quad x_i \leq \delta_1 : T_i^1 = T_p + \Delta t Q_1(x, 0)/c_1, \quad x_i > \delta_1 : T_i^1 = T_p.$$

For transition $t^{f-1} \rightarrow t^f$ ($f \geq 2$) the approximate form of Eq. (2.1) resulting

from the introduction of adequate differential quotients can be proposed

$$(4.1) \quad \begin{aligned} \frac{T_i^f - T_i^{f-1}}{\Delta t} + \tau_{qi} \frac{T_i^f - 2T_i^{f-1} + T_i^{f-2}}{(\Delta t)^2} &= a_i \frac{T_{i+1}^{f-1} - 2T_i^{f-1} + T_{i-1}^{f-1}}{h^2} \\ &+ a_i \tau_{Ti} \left(\frac{T_{i+1}^{f-1} - 2T_i^{f-1} + T_{i-1}^{f-1}}{\Delta t h^2} - \frac{T_{i+1}^{f-2} - 2T_i^{f-2} + T_{i-1}^{f-2}}{\Delta t h^2} \right) \\ &+ \frac{1}{c_i} Q_i^{f-1} + \frac{\tau_{qi}}{c_i} \left(\frac{\partial Q}{\partial t} \right)_i^{f-1}. \end{aligned}$$

After the mathematical manipulations one has

$$(4.2) \quad \begin{aligned} T_i^f &= \frac{\Delta t h^2 + 2\tau_{qi} h^2 - 2a_i \Delta t (\Delta t + \tau_{Ti})}{h^2 (\Delta t + \tau_{qi})} T_i^{f-1} - \frac{\tau_{qi} h^2 - 2a_i \Delta t \tau_{Ti}}{h^2 (\Delta t + \tau_{qi})} T_i^{f-2} \\ &+ \frac{a_i \Delta t (\Delta t + \tau_{Ti})}{h^2 (\Delta t + \tau_{qi})} (T_{i+1}^{f-1} + T_{i-1}^{f-1}) - \frac{a_i \Delta t \tau_{Ti}}{h^2 (\Delta t + \tau_{qi})} (T_{i+1}^{f-2} + T_{i-1}^{f-2}) \\ &+ \frac{(\Delta t)^2}{c_i (\Delta t + \tau_{qi})} \left[Q_i^{f-1} + \tau_{qi} \left(\frac{\partial Q}{\partial t} \right)_i^{f-1} \right]. \end{aligned}$$

This formula allows to calculate the temperatures at the internal nodes i . Let m_e , $e = 1, 2, \dots$, and $E - 1$ is the node located on the interfacial surface $x = L_e$, as shown in Fig. 2. The approximate form of boundary condition (3.5) can be taken in the following way:

$$(4.3) \quad \begin{aligned} &-\lambda_e \frac{T_{m_e}^f - T_{m_e-1}^f}{h} - \lambda_e (\tau_{Te} + \tau_{qe+1}) \frac{1}{\Delta t} \left(\frac{T_{m_e}^f - T_{m_e-1}^f}{h} - \frac{T_{m_e}^{f-1} - T_{m_e-1}^{f-1}}{h} \right) \\ &- \lambda_e \tau_{Te} \tau_{qe+1} \frac{1}{(\Delta t)^2} \left(\frac{T_{m_e}^f - T_{m_e-1}^f}{h} - 2 \frac{T_{m_e}^{f-1} - T_{m_e-1}^{f-1}}{h} + \frac{T_{m_e}^{f-2} - T_{m_e-1}^{f-2}}{h} \right) \\ &= -\lambda_{e+1} \frac{T_{m_e+1}^f - T_{m_e}^f}{h} - \lambda_{e+1} (\tau_{Te+1} + \tau_{qe}) \frac{1}{\Delta t} \left(\frac{T_{m_e+1}^f - T_{m_e}^f}{h} - \frac{T_{m_e+1}^{f-1} - T_{m_e}^{f-1}}{h} \right) \\ &- \lambda_{e+1} \tau_{Te+1} \tau_{qe} \frac{1}{(\Delta t)^2} \left(\frac{T_{m_e+1}^f - T_{m_e}^f}{h} - 2 \frac{T_{m_e+1}^{f-1} - T_{m_e}^{f-1}}{h} + \frac{T_{m_e+1}^{f-2} - T_{m_e}^{f-2}}{h} \right), \end{aligned}$$

hence

$$(4.4) \quad \begin{aligned} T_{m_e}^f &= \frac{A_{e1}}{A_{e1} + A_{e2}} T_{m_e-1}^f + \frac{A_{e2}}{A_{e1} + A_{e2}} T_{m_e+1}^f \\ &+ \frac{A_{e3}(T_{m_e}^{f-1} - T_{m_e-1}^{f-1}) + A_{e5}(T_{m_e}^{f-2} - T_{m_e-1}^{f-2})}{A_{e1} + A_{e2}} \\ &- \frac{A_{e4}(T_{m_e+1}^{f-1} - T_{m_e}^{f-1}) + A_{e6}(T_{m_e+1}^{f-2} - T_{m_e}^{f-2})}{A_{e1} + A_{e2}}, \end{aligned}$$

where

$$\begin{aligned}
 A_{e1} &= \lambda_e [(\Delta t)^2 + \Delta t(\tau_{Te} + \tau_{qe+1}) + \tau_{qe+1}\tau_{Te}], \\
 A_{e2} &= \lambda_{e+1} [(\Delta t)^2 + \Delta t(\tau_{Te+1} + \tau_{qe}) + \tau_{qe}\tau_{Te+1}], \\
 (4.5) \quad A_{e3} &= \lambda_e [\Delta t(\tau_{Te} + \tau_{qe+1}) + 2\tau_{qe+1}\tau_{Te}], \\
 A_{e4} &= \lambda_{e+1} [\Delta t(\tau_{Te+1} + \tau_{qe}) + 2\tau_{qe}\tau_{Te+1}], \\
 A_{e5} &= -\lambda_e \tau_{qe+1}\tau_{Te}, \quad A_{e6} = -\lambda_{e+1}\tau_{qe}\tau_{Te+1}.
 \end{aligned}$$

In turn, for the nodes 0 ($x = 0$) and n ($x = L$) (cf. boundary conditions (3.6)) one has

$$\begin{aligned}
 (4.6) \quad \frac{T_1^f - T_0^f}{h} + \tau_{T1} \frac{1}{\Delta t} \left(\frac{T_1^f - T_0^f}{h} - \frac{T_1^{f-1} - T_0^{f-1}}{h} \right) &= 0, \\
 \frac{T_n^f - T_{n-1}^f}{h} + \tau_{TE} \frac{1}{\Delta t} \left(\frac{T_n^f - T_{n-1}^f}{h} - \frac{T_n^{f-1} - T_{n-1}^{f-1}}{h} \right) &= 0,
 \end{aligned}$$

it means that

$$\begin{aligned}
 (4.7) \quad T_0^f &= T_1^f - \frac{\tau_{T1}}{\Delta t + \tau_{T1}} (T_1^{f-1} - T_0^{f-1}), \\
 T_n^f &= T_{n-1}^f + \frac{\tau_{TE}}{\Delta t + \tau_{TE}} (T_n^{f-1} - T_{n-1}^{f-1}).
 \end{aligned}$$

Because the explicit scheme of the finite difference method is proposed here, therefore the stability criteria should be formulated (see [16, 17]).

5. Results of computations

As an example, a double-layered thin film (gold and chromium) subjected to a laser pulse is considered. The thicknesses of layers are equal to 50 nm. The initial temperature is equal to $T_{e0} = 300$ K. In Table 1 the thermophysical parameters of materials are collected [18, 19].

Table 1. Thermophysical parameters.

	Gold	Chromium
Volumetric specific heat [MJ/(m ³ ·K)]	$c_1 = 2.4897$	$c_2 = 3.21484$
Thermal conductivity [W/(m·K)]	$\lambda_1 = 315$	$\lambda_2 = 93$
Relaxation time [ps]	$\tau_{q1} = 8.5$	$\tau_{q2} = 0.136$
Thermalization time [ps]	$\tau_{T1} = 90$	$\tau_{T2} = 7.86$
Reflectivity	$R_1 = 0.95$	$R_2 = 0.974$
Absorption depth [nm]	$\delta_1 = 15.3$	$\delta_2 = 15.3$

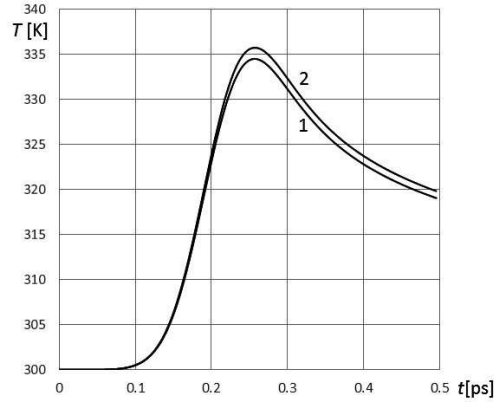


FIG. 3. Temperature history at the irradiated surface: 1 – $n = 100$, $\Delta t = 2 \cdot 10^{-4}$ ps, 2 – $n = 1000$, $\Delta t = 2 \cdot 10^{-6}$ ps.

The computations are performed for the laser intensity $I_0 = 40 \text{ W/m}^2$ and the characteristic time of the laser pulse $t_p = 0.1 \text{ ps}$ (cf. formula (2.2)). In Fig. 3 the temperature history at the irradiated surface for $n = 100$, $\Delta t = 2 \cdot 10^{-4}$ ps and $n = 1000$, $\Delta t = 2 \cdot 10^{-6}$, respectively, is shown. Because the results are grid independent for $n \geq 1000$, so in the further calculations $n = 1000$ nodes is assumed.

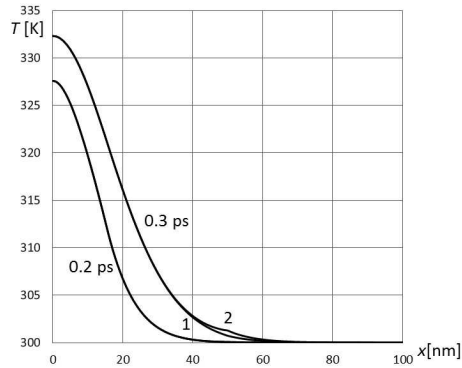


FIG. 4. Temperature distribution for 0.2 and 0.3 ps (1 – DPL model, 2 – DPL with the macroscopic boundary conditions).

In Figs. 4–6 the temperature profiles for times 0.2, 0.3, 0.4 and 0.5 ps are shown. The curves marked as 1 correspond to the solution of DPL equation (2.1) with the boundary conditions (3.5), (3.6), while the curves marked as 2 illustrate the solution of the same equation supplemented by the classical macroscopic

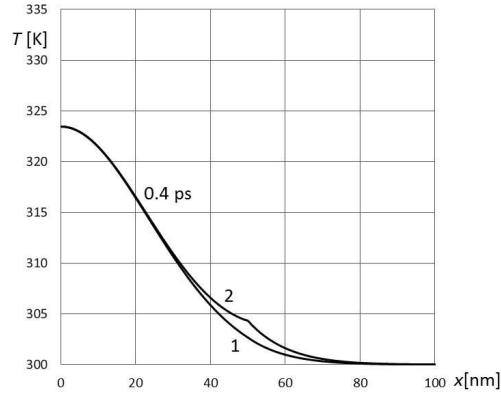


FIG. 5. Temperature distribution for 0.4 ps (1 – DPL model, 2 – DPL with the macroscopic boundary conditions).

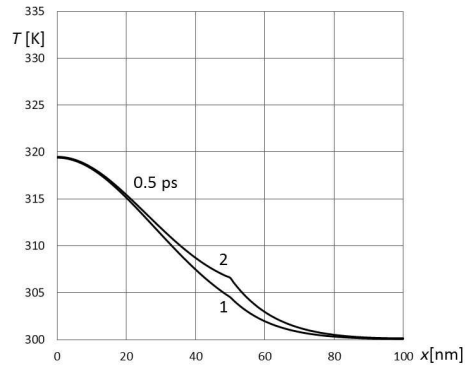


FIG. 6. Temperature distribution for 0.5 ps (1 – DPL model, 2 – DPL with the macroscopic boundary conditions).

continuity conditions (in equations (3.5), (3.6): $\tau_{qe} = 0$ and $\tau_{Te} = 0$). It can be seen that over time the temperature differences increase especially in the vicinity of the contact surface.

Figure 7 illustrates the temperature courses on the contact surface between the layers for the DPL model (curve 1) and the DPL model with the macroscopic boundary conditions (curve 2). After 0.5 ps the maximum temperature on the contact surface is equal to 304.29 K and 306.35 K, respectively.

In Fig. 8, the temperature history at the irradiated surface for both cases is presented. The differences between the temperatures are small (temperatures for time 0.5 ps are equal to 319.84 K and 319.92 K, respectively), which shows that in the case of the Neumann boundary condition (cf. equation (3.6)) the assumption that $\tau_{T1} = 0$ is acceptable.

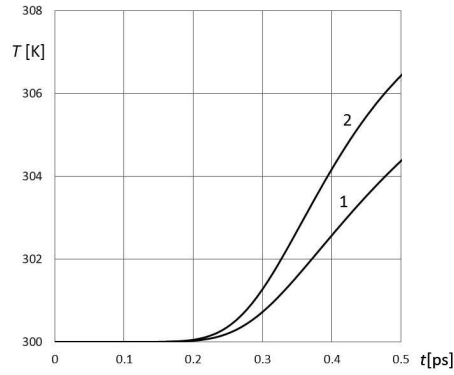


FIG. 7. Temperature courses on the contact surface (1 – DPL model, 2 – DPL with the macroscopic boundary conditions).

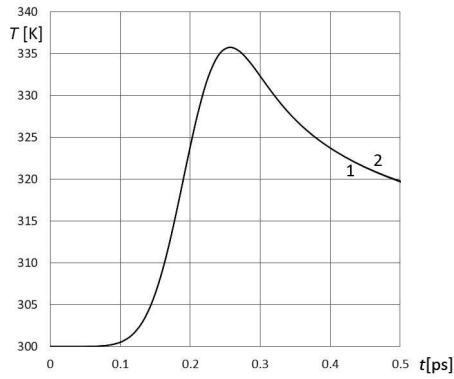


FIG. 8. Temperature courses on the irradiated surface (1 – DPL model, 2 – DPL supplemented by the macroscopic boundary conditions).

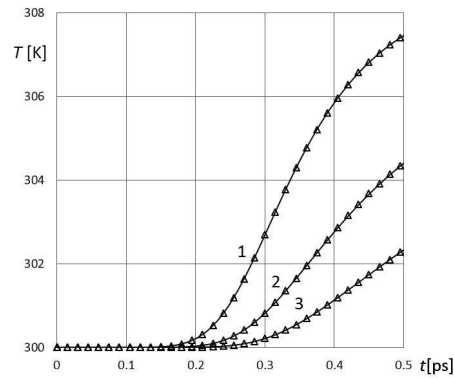


FIG. 9. Temperature courses at points 1–40 nm, 2–50 nm, 3–60 nm, solid lines – one layer, symbols – two layers.

To check the correctness of the ideal contact modeling the following problem has been analyzed. In the first version, the layer of thickness L made of gold is considered, while in the second version two layers of thicknesses $L/2$ made of the same material (gold) are taken into account. Between these layers the condition corresponding to the ideal thermal contact (3.5) is assumed. It turned out that the same solutions were obtained, what is shown in Fig. 9. So the analytical form of condition (3.5) and its numerical realization are definitely correct. It should be noted that when using the dual-phase lag equation for numerical modeling of thermal processes occurring in the heated metal films

the physical anomalies can take place [20–22]. They are connected with the values of the delay times τ_q and τ_T [23]. When $\tau_T > \tau_q$ (cf. Table 1) the DPL model might violate the second law of thermodynamics and this case is defined as over-diffusion [20, 24]. Such phenomena, however, can be explained by the non-equilibrium entropy production theory [25]. The interpretation of this phenomenon, from a mathematical point of view, can be also found in [20]. On the other hand, the thermalization time τ_T and the relaxation time τ_q are the intrinsic properties of the material in question and in the literature one can find a lot of papers connected with the ultrafast pulse-laser heating on metal films related to the case $\tau_q < \tau_T$, e.g., [5–11, 14–19]. Moreover, the calculations show very good agreement with the experimental results [7, 24].

6. Conclusions

A dual-phase lag model describing the thermal processes occurring in the multilayered thin metal film subjected to the ultrashort laser pulse is considered. The ideal contact conditions at the interfaces between the layers are formulated according to the formula describing the dependence between the heat flux and temperature gradient in which the phase lag times are taken into account. To solve this problem the explicit scheme of the finite difference method is proposed. The results of computations show that the condition of ideal contact assumed in the same manner as in the case of macroscopic Fourier model is a significant simplification.

Presented in this paper, formulation of ideal contact condition supplementing the dual-phase lag model can be used in the case of other numerical methods, e.g. the general boundary element method [26–28] or analytical methods [29–31].

Acknowledgements

The paper and research were financed within the project 2015/19/B/ST8/01101 sponsored by the National Science Centre (Poland).

References

1. D.Y. TZOU, *Macro- to Microscale Heat Transfer. The lagging behavior*, Taylor and Francis, 1997.
2. Z.M. ZHANG, *Nano/Microscale Heat Transfer*, McGraw-Hill, New York, 2007.
3. A.N. SMITH, P.M. NORRIS, [in:] *Heat Transfer Handbook*, Adrian Bejan [Ed.], John Wiley & Sons: Hoboken, 1309–1409, 2003.
4. G. CHEN, D. BORCA-TASCIUC, R.G. YANG, [in:] *Encyclopedia of Nanoscience and Nanotechnology*, Hari Singh Nalwa [Ed.], American Scientific Publishers: Stevenson Ranch, **7**, 429–459, 2004.
5. E. MAJCHRZAK, B. MOCHNACKI, *Sensitivity analysis of transient temperature field in microdomains with respect to the dual phase lag model parameters*, International Journal for Multiscale Computational Engineering, **12**, 1, 65–77, 2014.
6. B. MOCHNACKI, M. PARUCH, *Estimation of relaxation and thermalization times in microscale heat transfer model*, Journal of Theoretical and Applied Mechanics, **51**, 4, 837–845, 2013.
7. E. MAJCHRZAK, B. MOCHNACKI, A.L. GREER, J.S. SUCHY, *Numerical modeling of short pulse laser interactions with multi-layered thin metal films*, CMES: Computer Modeling in Engineering and Sciences, **41**, 2, 131–146, 2009.
8. E. MAJCHRZAK, B. MOCHNACKI, J.S. SUCHY, *Numerical simulation of thermal processes proceeding in a multi-layered film subjected to ultrafast laser heating*, Journal of Theoretical and Applied Mechanics, **47**, 2, 383–396, 2009.
9. E. MAJCHRZAK, Ł. TURCHAN, J. DZIATKIEWICZ, *Modeling of skin tissue heating using the generalized dual-phase lag equation*, Archives of Mechanics, **67**, 6, 417–437, 2015.
10. H. WANG, W. DAI, R. MELNIK, *A finite difference method for studying thermal deformation in a double-layered thin film exposed to ultrashort pulsed lasers*, International Journal of Thermal Sciences, **45**, 1179–1196, 2006.
11. H. WANG, W. DAI, L.G. HEWAVITHARANA, *A finite difference method for studying thermal deformation in a double-layered thin film with imperfect interfacial contact exposed to ultrashort pulsed lasers*, International Journal of Thermal Sciences, **47**, 7–24, 2008.
12. S. SINGH, S. KUMAR, *Numerical study on triple layer skin tissue freezing using dual phase lag bio-heat model*, International Journal of Thermal Sciences, **86**, 12–20, 2014.
13. S. SINGH, S. KUMAR, *Numerical analysis of triple layer skin tissue freezing using non-Fourier heat conduction*, Journal of Mechanics in Medicine and Biology, **16**, 2, 1650017, 2015.
14. J.K. CHEN, J.E. BERAUN, *Numerical study of ultrashort laser pulse interactions with metal films*, Numerical Heat Transfer, Part A, **40**, 1–20, 2001.
15. J.R. HO, CH. P. KUO, W.S. JIAUNG, *Study of heat transfer in multilayered structure within the framework of dual-phase-lag heat conduction model using lattice Boltzmann method*, International Journal of Heat and Mass Transfer, **46**, 55–69, 2003.
16. J.M. McDONOUGH, I. KUNADIAN, R.R. KUMAR, T. YANG, *An alternative discretization and solution procedure for the dual phase-lag equation*, Journal of Computational Physics, **219**, 163–171, 2006.
17. E. MAJCHRZAK, B. MOCHNACKI, *Dual-phase lag equation. Stability conditions of a numerical algorithm based on the explicit scheme of the finite difference method*, Journal of Applied Mathematics and Computational Mechanics, **15**, 3, 89–96, 2016.

18. W. DAI, R. NASSAR, *A domain decomposition method for solving three-dimensional heat transport equations in a double-layered thin film with microscale thickness*, Numerical Heat Transfer, Part A, **38**, 243–255, 2000.
19. A. KARAKAS, M. TUNC, U. CAMDALI, *Thermal analysis of thin multi-layer metal films during femtosecond laser heating*, Heat and Mass Transfer, **46**, 1287–1293, 2010.
20. B. SHEN, P. ZHANG, *Notable physical anomalies manifested in non-Fourier heat conduction under the dual-phase-lag model*, International Journal of Heat and Mass Transfer, **51**, 1713–1727, 2008.
21. M. WANG, N. YANG, Z.-Y. GUO, *Non-Fourier heat conductions in nanomaterials*, Journal of Applied Physics, **110**, 064310, 7 pp., 2011 (doi:http://dx.doi.org/10.1063/1.3634078).
22. S.A. RUKOLAINE, *Unphysical effects of the dual-phase-lag model of heat conduction*, International Journal of Heat and Mass Transfer, **78**, 58–63, 2014.
23. M. FABRIZIO, B. LAZZARI, *Stability and second law of thermodynamics in dual-phase-lag heat conduction*, International Journal of Heat and Mass Transfer, **74**, 484–489, 2014.
24. D.W. TANG, N. ARAKI, *Wavy, wavelike, diffusive thermal responses of finite rigid slabs to high-speed heating of laser-pulses*, International Journal of Heat and Mass Transfer, **42**, 855–860, 1999.
25. M.A. AL-NIMR, M. NAJI, V.S. ARBACI, *Nonequilibrium entropy production under the effect of the dual-phase-lag heat conduction model*, ASME Journal of Heat Transfer, **122**, 217–223, 2000.
26. E. MAJCHRZAK, *Numerical solution of dual phase lag model of bioheat transfer using the general boundary element method*, CMES: Computer Modeling in Engineering and Sciences, **69**, 1, 43–60, 2010.
27. E. MAJCHRZAK, Ł. TURCHAN, *The general boundary element method for 3D dual-phase lag model of bioheat transfer*, Engineering Analysis with Boundary Elements, **50**, 76–82, 2015.
28. B. YU, W.A. YAO, H.L. ZHOU, H.L. CHEN, *Precise time-domain expanding BEM for solving non-Fourier heat conduction problems*, Numerical Heat Transfer Problems, Part B – Fundamentals, **68**, 6, 511–532, 2015.
29. B.S. YILBAS, A.Y. AL-DWEIK, *Exact solution for temperature field due to non-equilibrium heating of solid substrate*, Physica B, **406**, 4523–4528, 2011.
30. J. ESCOLANO, F. RODRÍGUEZ, M.A. CASTRO, F. VIVES, J.A. MARTÍN, *Exact and analytic-numerical solutions of bidimensional lagging models of heat conduction*, Mathematical and Computer Modeling, **54**, 7–8, 1841–1845, 2011.
31. H. ASKARIZADEH, H. AHMADIKIA, *Analytical analysis of the dual-phase-lag heat transfer equation in a finite slab with periodic surface heat flux*, International Journal of Engineering, **27**, 6, 971–978, 2014.

Received September 28, 2016; revised version November 26, 2016.